Contemporary crustal deformation around the southeast borderland of the Tibetan Plateau

Zheng-Kang Shen,[1,2] Jiangning Lü,[3] Min Wang,[4] and Roland Bürgmann,[5]

Received 3 September 2004; revised 7 July 2005; accepted 30 August 2005; published XX Month 2005.

[1] We derive a detailed horizontal velocity field for the southeast borderland of the Tibetan Plateau using GPS data collected from the Crustal Motion Observation Network of China between 1998 and 2004. Our results reveal a complex deformation field that indicates that the crust is fragmented into tectonic blocks of various sizes, separated by strike-slip and transtensional faults. Most notably, the regional deformation includes 10–11 mm/yr left slip across the Xianshuihe fault, ~7 mm/yr left slip across the Anninghe-Zemuhe-Xiaojiang fault zone, ~2 mm/yr right slip across a shear zone trending northwest near the southern segment of the Lancang River fault, and ~3 mm/yr left slip across the Lijiang fault. Deformation along the southern segment of the Red River fault appears not significant at present time. The region south and west of the Xianshuihe-Xiaojiang fault system, whose eastward motion is resisted by the stable south China block to the east, turns from eastward to southward motion with respect to south China, resulting in clockwise rotation of its internal subblocks. Active deformation is detected across two previously unknown deformation zones: one is located ~150 km northwest of and in parallel with the Longmenshan fault with 4–6 mm/yr right-slip and another is continued south-southwestward from the Xiaojiang fault abutting the Red River fault with ~7 mm/yr left slip. While both of these zones are seismically active, the exact locations of faults responsible for such deformation are yet to be mapped by field geology. Comparing our GPS results with predictions of various models proposed for Tibetan Plateau deformation, we find that the relatively small sizes of the inferred microblocks and their rotation pattern lend support to a model with a mechanically weak lower crust experiencing distributed deformation underlying a stronger, highly fragmented upper crust.

Citation: Shen, Z.-K., J. Lü, M. Wang, and R. Bürgmann (2005), Contemporary crustal deformation around the southeast borderland of the Tibetan Plateau, *J. Geophys. Res.*, *110*, XXXXXX, doi:10.1029/2004JB003421.

1. Introduction

[2] The southeast borderland of the Tibetan Plateau is located between the heartland of the plateau to the west and the stable south China block to the east (Figure 1). It spans most of Sichuan and Yunnan provinces in southwest China, and is characterized by complex Cenozoic structures created during the Indo-Asia collision process [e.g., *Molnar and Tapponnier*, 1975; *Yin and Harrison*, 2000]. Over the past three decades various models have been developed to describe the tectonic evolution and uplift of the Tibetan Plateau, following the ground breaking work of *Molnar and Tapponnier* [1975] [e.g., *England and McKenzie*, 1982; *Tapponnier et al.*, 1982, 2001; *Vilotte et al.*, 1986; *Peltzer and Tapponnier*, 1988; *Houseman and England*, 1986, 1993, 1996; *Holt et al.*, 1995, 2000; *Kong and Bird*, 1996; *Royden et al.*, 1997; *England and Molnar*, 1997a, 1997b; *Flesch et al.*, 2001; *F. Shen et al.*, 2001; *Replumaz and Tapponnier*, 2003]. Differences between these models usually focus on two important questions: (1) Is tectonic deformation block-like or broadly distributed? (2) Is the north-south shortening of the Tibetan Plateau absorbed mainly by crustal thickening or eastward extrusion? One school of thought believes that the collision zone is composed of a collage of lithospheric blocks and deformation takes place mainly along block boundaries delineated by large-scale, rapidly slipping strike-slip faults. Because the blocks cannot absorb deformation internally, in this view north-south shortening of the Tibetan Plateau is accommodated by rapid eastward extrusion [*Tapponnier et al.*, 1982; *Peltzer and Tapponnier*, 1988; *Avouac and Tapponnier*, 1993]. Another school suggests that the crustal strength is reduced by the existence of a ductile lower crust, making deformation between the upper crust and mantle "decoupled". Therefore northward advancement of the

[1]State Key Laboratory of Earthquake Dynamics, Institute of Geology, China Earthquake Administration, Beijing, China.
[2]Also at Department of Earth and Space Sciences, University of California, Los Angeles, California, USA.
[3]Department of Geophysics, Peking University, Beijing, China.
[4]Institute of Earthquake Science, China Earthquake Administration, Beijing, China.
[5]Department of Earth and Planetary Science, University of California, Berkeley, California, USA.

0148-0227/05/2004JB003421$09.00

Indian plate results in thickening of the lower crust and broadly distributed deformation [*England and McKenzie*, 1982; *Vilotte et al.*, 1986; *Houseman and England*, 1996]. Mechanically speaking, the block models suggest an important role of high slip rate, deeply rooted strike-slip faults bounding major blocks, while the ''decoupled'' models advocate that such faults are likely to be slow and abundant, reflecting a regional crustal flow field, preexisting weaknesses, and driving stress conditions. These two groups of end-member models suggest rather different crustal deformation patterns in the vicinity of the plateau, particularly around its east and southeast borderland (e.g.,

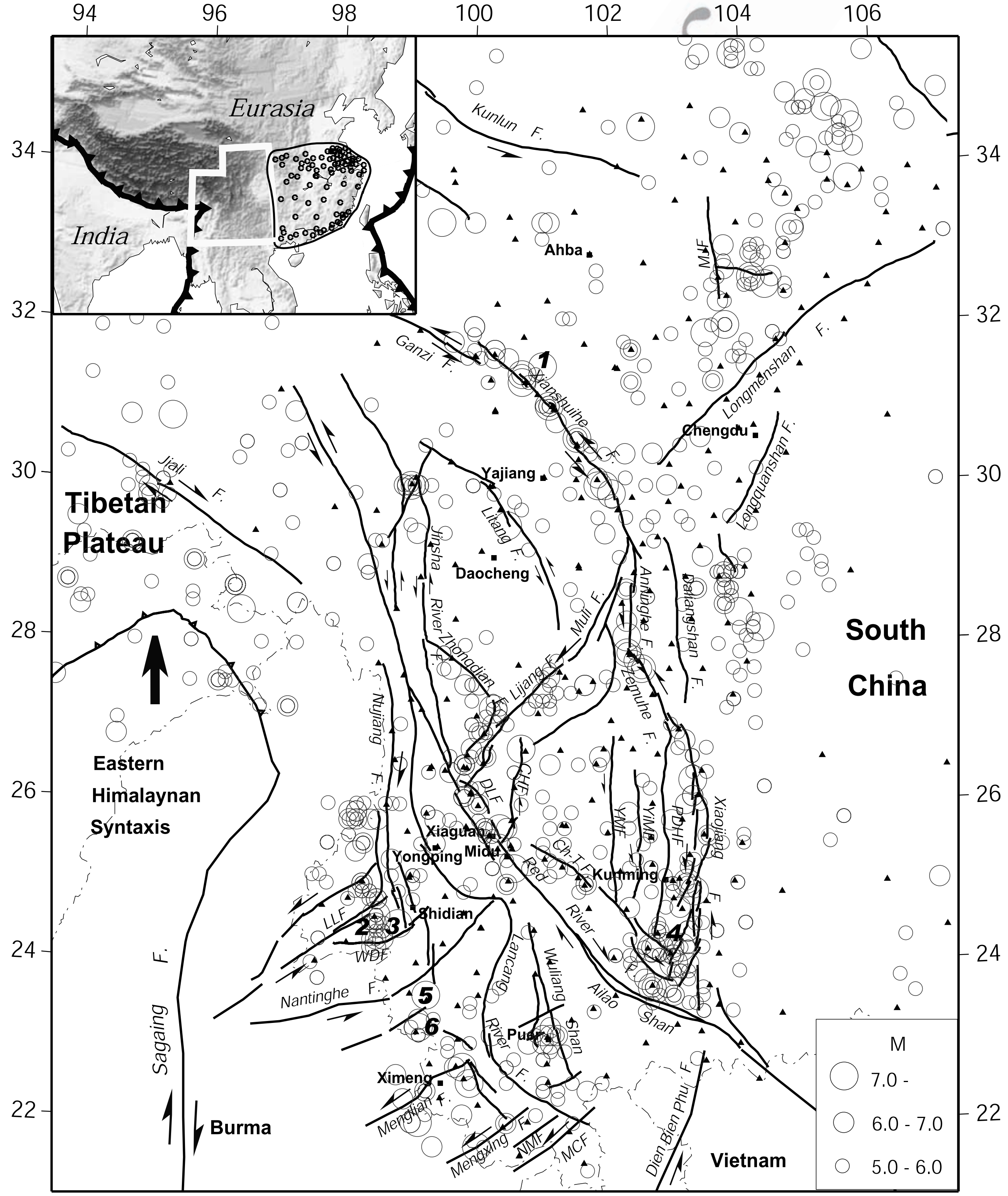

Figure 1

Replumaz and Tapponnier's [2003] Figure 3 versus *F. Shen et al.*'s [2001] Plate 2). Thus precise measurement of crustal deformation patterns in this region is crucial in differentiating these kinematic and geodynamic models.

[3] In the last decade, space geodetic techniques, especially the Global Positioning System (GPS) have been used successfully to measure the crustal motion across tectonic deformation zones. Such studies in the Tibetan Plateau and its vicinity have provided us with a basic understanding of crustal deformation patterns in the region [*Bilham et al.*, 1997; *King et al.*, 1997; *Larson et al.*, 1999; *Chen et al.*, 2000; *Z.-K. Shen et al.*, 2001; *Wang et al.*, 2001; *Vigny et al.*, 2003; *Chen et al.*, 2004; *Zhang et al.*, 2004]. GPS data have been used to argue against [e.g., *Zhang et al.*, 2004] and for (W. Thatcher, submitted to *Science*, 2005) block-like deformation of the Tibetan Plateau. Still, densified GPS station networks are needed to acquire more precise measurements of contemporary crustal deformation in key regions such as the southeast borderland, in order to provide stronger constraints on the kinematics of deformation of the Tibetan Plateau and its adjoining regions.

[4] Independent of the preferred geodynamic model of the region, upper crustal deformation is brittle and discontinuous and affected by earthquake cycle effects. Throughout much of the earthquake cycle (the so-called interseismic period) deformation is essentially steady in time and elastic strain is concentrated within 2–3 locking depths of crustal faults [e.g., *Thatcher*, 1983]. In the years following a large crustal earthquake, deformation rates are accelerated by various postseismic relaxation processes, which decay to background levels within a few decades [e.g., *Thatcher*, 1983]. Thus, unless a large ($M > 7$) earthquake occurred within the last decade or two, widely spaced geodetic measurements across a fault zone are expected to reflect long-term rates. Dense geodetic measurements are needed to delineate high strain rate zones associated with major faults and identify essentially rigid block interiors. If the deformation is well explained by horizontal motions of large, undeforming blocks, a lithospheric extrusion model may be favored. In this case, faults are expected to be long-lived features of localized deformation throughout the lithosphere. If the dimensions of inferred crustal tectonic blocks in a broadly distributed deformation zone is less than a few hundreds kilometers and slip rates are low, we may infer that deformation at depth occurs by broadly distributed flow. It can be argued, however, that as block dimensions decrease, the two types of models converge. In addition to these block dimension aspects, geodynamic models of continental deformation predict different first-order patterns of deformation, such as the nature of rotation about the eastern syntaxis of the Himalaya that may provide further diagnostic evidence. In continuum flow models, slip rates and the distribution of active faults may vary relatively rapidly through geologic time. Ultimately, the debate about the nature of continental deformation in the Indo-Eurasian collision zone is about the rheology and localization of deformation in the lower crust and upper mantle.

[5] In this study, following a brief overview of major fault zones in the region we present the horizontal velocity field in the southeast borderland of Tibet inferred from GPS. We then derive kinematic parameters of major tectonic structures in the framework of rigidly rotating crustal blocks separated by active faults. Finally, we compare our result with results and predictions of previous studies and discuss implications of our new findings regarding the crustal deformation along the eastern margin of the Tibetan Plateau.

2. Geological Setting

[6] Deformation of the southeast borderland of the Tibetan Plateau is thought to have intensified since the late Tertiary as uplift and deformation associated with the Indo-Eurasian collision accelerated in the region [*Replumaz et al.*, 2001; *Wang and Burchfiel*, 2000; *Xu and Kamp*, 2000]. The borderland is sliced by a network of tectonic faults, among which the Xianshuihe-Xiaojiang fault system is the most active (Figure 1) [*Wang et al.*, 1998]. This fault system is composed of, from north to south, the Xianshuihe fault striking northwest, the Anninghe fault trending nearly north, the Zemuhe fault trending north-northwest, and the Xiaojiang fault striking nearly north-south [*Kan*, 1977; *Li and Wang*, 1977; *Allen et al.*, 1991; *Wang et al.*, 1998]. The entire fault system is about 1200 km long and a few hundred meters wide in most places, except across the mid and southern parts of the Xiaojiang fault where it splits into multiple branches spanning a range of 20–30 km. The fault system was incepted from at least late Pliocene to early Quaternary (~4–2 Ma) [*Wang et al.*, 1998] and is seismically active at present: 14 $M > 7.0$ earthquakes were recorded historically since 814, including an event of $M = 8.0$ in 1833 [*Zhang and Xie*, 2001], with a maximum focal depth of ~20 km [*Tang et al.*, 1993]. Two $M > 7$ events occurred along the fault system during the last century: the 1973 *M*7.5 Luhuo earthquake struck the central section of the Xianshuihe fault, and the 1970 *M*7.3 Tonghai earthquake took place near the intersection of the Xiaojiang and Red River-Ailao Shan fault systems [*Holt et al.*, 1995] (Figure 1). Across a pull-apart basin the Xian-

Figure 1. Tectonic map of southeast borderland of Tibetan Plateau [after *Wang et al.*, 1998; *Lacassin et al.*, 1998; *Chen et al.*, 2000; *Wang and Burchfiel*, 2000; *Deng et al.*, 2003]. The study area is depicted in the inset map. Dots in the inset map show stations used to define the south China reference frame (delineated by the solid curve). Triangles denote the GPS survey stations. Circles are earthquakes from 780 B.C. to 1996 [*Division of Earthquake Monitoring and Prediction, State Seismological Bureau*, 1995; *Division of Earthquake Monitoring and Prediction, China Seismological Bureau*, 1999]. The events of $M \geq 7$ occurred in the 20th century are marked with italic numbers: 1, 1973 *M*7.5 Luhuo; 2, 1976 *M*7.0 Shidian; 3, 1976 *M*7.1 Longling; 4, 1970 *M*7.3 Tonghai; 5, 1988 *M*7.0 Lancang; and 6, 1988 *M*7.1 Gengma earthquakes [*Holt et al.*, 1995]. Abbreviations are Ch-T Flt., Chuxiong-Tonghai fault; CHF, Chenghai fault; LLF, Longling fault; MCF, Mae Chan fault; MJF, Minjiang fault; NMF, Nam Ma fault; PDHF, Puduhe fault; WDF, Wanding fault; YiMF, Yimen fault; YMF, Yuanmou fault.

shuihe fault system continues northwesterly as the Ganzi fault, and about 150 km southwest of and in parallel with the Xianshuihe fault lies the Litang fault. All of the faults slip left laterally and are usually situated in deeply incised valleys separating high mountain ranges in between [*Ma*, 1989; *Wang and Burchfiel*, 2000].

[7] South of the Xianshuihe-Xiaojiang fault system lies the Red River-Ailao Shan shear zone, which is a major physiographic and geological discontinuity in East Asia. It is unmistakably visible on satellite images with a sharply defined fault zone and narrow trough, stretching for more than 1000 km from Tibet to the Hanoi basin [*Allen et al.*, 1984; *Tapponnier et al.*, 1990; *Leloup et al.*, 1995]. It has long been presented as a classic example of a lithospheric-penetrative, intracontinental transform fault, separating the Indochina block from the south China block [e.g., *Tapponnier and Molnar*, 1977; *Allen et al.*, 1984; *Leloup et al.*, 2001]. Four metamorphic massifs, the Xuelong Shan, Diancang Shan, Ailao Shan (in Yunnan, China), and Day Nui Con Voi (in Vietnam), are exposed as 10–20 km wide belts of high-grade metamorphic rocks along the fault [*Leloup et al.*, 1995, 2001]. Abundant geochronological and thermobarometric evidence has been presented for late Tertiary (∼35–17 Ma) ductile, left-lateral shearing of about 700 ± 200 km along the Red River-Ailao Shan shear zone [e.g., *Tapponnier et al.*, 1990; *Schärer et al.*, 1990; *Harrison et al.*, 1992, 1996; *Leloup et al.*, 1995, 2001; *Zhang and Schärer*, 1999; *Burchfiel and Wang*, 2003; *Gilley et al.*, 2003]. The opening of the south China Sea (30.5–17 Ma) [*Briais et al.*, 1993] was probably driven by left-lateral strike-slip faulting on the Red River-Ailao Shan shear zone [e.g., *Tapponnier et al.*, 1982; *Harrison et al.*, 1996; *Leloup et al.*, 2001]. The left-slip motion was reversed to right-lateral slip on the Red River-Ailao Shan shear zone ∼4.5 Ma [e.g., *Leloup et al.*, 1995; *Harrison et al.*, 1996; *Wang et al.*, 1998]. Total right-lateral offset is estimated between ∼6 and ∼60 km [*Allen et al.*, 1984; *Leloup et al.*, 1995; *Wang et al.*, 1998; *Replumaz et al.*, 2001]. South of the Red River fault, strands of northeast striking left-lateral faults, such as the Dien Bien Phu, Mae Chan, Nam Ma, Mengxing, and Menglian faults, are present, but do not seem to reach up to the Red River fault. The Red River fault appears to truncate the southward extension of the left-slip Xianshuihe-Xiaojiang fault system in a complex zone of distributed faulting [*Le Dain et al.*, 1984; *Wang and Burchfiel*, 1997; *Lacassin et al.*, 1998].

[8] At its northwest end, the Red River fault system connects to the Dali fault, and merges into a group of north-south trending faults such as the Jinsha River and Lancang River faults (Figure 1). The Jinsha River, Lancang River, and Nujiang faults are near parallel at 27–30° latitude. To the south, the three faults spread out into a complex fault system: The Nujiang fault splits into a group of faults trending northeast, represented by the Longling fault. This fault system has been seismically active for the past several decades, and experienced two magnitude 7 events in 1976 (Figure 1). The Lancang River fault bends counterclockwise and splits into the Nantinghe, south Lancang River, and Wuliang Shan faults trending northeast, NNE, and northwest, respectively. The M_w 7.1 Lancang and M_w 7.0 Gengma earthquakes occurred along the Nandinghe fault system in 1988 (Figure 1). The Jinsha River fault extends southeastward to merge into the Red River and Dali fault system [*Institute of Geology et al.*, 1990; *Wang et al.*, 1998; *Deng et al.*, 2003]. Further south, the faults become unclear and distributed in the northern mountains of Indochina. The region bounded by the Xianshuihe-Xiaojiang, Red River, and Jinsha River fault systems is usually considered as a tectonic terrane, called the Sichuan-Yunnan fragment [*Kan*, 1977; *Li and Wang*, 1977; *Wang et al.*, 1998]. Crustal motion of the region is predominantly clockwise rotation around the eastern Himalayan Syntaxis (EHS), transporting the plateau material from eastward motion north of the syntaxis to southward motion east of it with respect to south China.

[9] In the region north of the Xianshuihe fault, the topographic margin of the Tibetan Plateau along the Longmen Shan is one of the most striking continental escarpments on Earth: Elevation rises from ∼500 m in the Sichuan Basin to peaks exceeding 6500 m over a horizontal distance of ∼50 km. Active faults which have been mapped in this region, however, are scant, and appear to be restricted to the Minshan and Longmenshan fault zones [*Chen et al.*, 1994; *Tang et al.*, 1995; *Burchfiel et al.*, 1995]. Epicenters of contemporary earthquakes are scattered in a region northwest of the Longmenshan fault, within which a seismic zone trending NNE is vaguely visible (Figure 1).

3. GPS Data and Processing

[10] GPS data used in this study are mainly from the Crustal Motion Observation Network of China (CMONOC [*Ma et al.*, 2001; *M. Wang et al.*, 2003; *Zhang et al.*, 2004]) project. They include data from a nationwide fiducial network of 25 continuous sites observed from July 1998 to October 2004, and 56 survey mode sites with yearly occupations 1998–2004. They also include more than 200 regional survey mode stations occupied in 1999, 2001, and 2004. All the survey mode sites were observed continuously for at least 4 days during each session. The GPS data were analyzed in three steps [*Shen et al.*, 2000]. First, the GPS carrier phase data were processed to obtain loosely constrained daily solutions for station positions and satellite orbits using the GAMIT software [*King and Bock*, 2000]. Second, the regional daily solutions were combined with global solutions produced by the Scripps Orbital and Position Analysis Center (SOPAC, http://sopac.ucsd.edu/) using the GLOBK software [*Herring*, 2002]. Third, the station positions and velocities were estimated through a Kalman filter procedure using the QOCA software (http://gipsy.jpl.nasa.gov/qoca/). The velocity solution is with respect to the global reference frame ITRF2000-NNR [*Altamimi et al.*, 2002], which is realized by carefully selecting a group of 16 global IGS sites (7 in North America, 3 in Australia, 4 in Eurasia, 1 in Pacific, and 1 in Antarctica) and constraining their velocities to the ITRF2000-NNR values at the uncertainties of 2, 2, and 5 mm/yr for their east, north, and up components, respectively. The velocity field can be transformed into regional reference frames (e.g., with respect to the Eurasian plate or south China block) by applying constraints that minimize the motions within the stable interior of these blocks. In a previous study, *M. Wang et al.* [2003] reported data analysis results of the entire CMONOC network and its preliminary

interpretations. A portion of the data has been used in *Zhang et al.* [2004] to analyze tectonic deformation in the Tibetan Plateau and its vicinities. Here, we focus on a detailed analysis and interpretation of the regional deformation field around the southeast borderland of the Tibetan Plateau, and the velocity data set is provided as an electronic supplement[1] to this paper.

4. Microblock Motion Model

[11] In the following analysis we assume that upper crustal deformation is block-like. That is, the region is divided into rigid blocks, which move with respect to each other in the form of translation and rotation. These blocks are delineated by active faults, which accommodate the deformation associated with relative block motions. It is necessary to point out that our microblock model differs from the block motion model mentioned in the introduction of this paper, in which large blocks are separated by a limited number of large, lithospheric strike-slip faults. As in both the distributed deformation and block motion models upper crustal deformation is still meant to be brittle and discontinuous, our kinematic model results can provide support for either view depending on the sizes of the blocks, the kind of faults delineating the block boundaries, and the overall pattern of regional deformation we infer.

[12] In our model we do not explicitly account for elastic deformation along block boundaries that is associated with locking of the brittle part of the faults [e.g., *Meade and Hager*, 2005]. For crustal strike-slip faults, such deformation takes place within ~30 km of the fault. Simple dislocation models show that ~70% and ~80% of elastic deformation take place within 30 km of a strike-slip fault locked at 15 and 10 km depth, respectively [e.g., *Savage and Burford*, 1970]. The blocks we consider are much larger than 30 km, making it possible to use the GPS sites located in the stable interior of the blocks to determine their relative motions. Given the 1–2 mm/yr precisions of our GPS velocities, we are only able to define relative motions and block stability at this level. Thus additional faults and block fragmentation at mm/yr rates or less are permitted by our analysis.

[13] In our model the postseismic deformation effect is not explicitly modeled either. Such an effect is usually negligible because the earthquakes are usually too small or occurred too long ago. The only events which might be able to produce detectable deformation and affect the GPS observations of this study are the 6 $M \geq 7$ events of the last century shown in Figure 1. Among these 6 events, 4 occurred more than 20 years before the start of the GPS measurements used in this study, by then most of the postseismic deformation is believed to have decayed to submillimeters per year levels. The other two events, the 1988 M_w 7.1 Lancang and M_w 7.0 Gengma earthquakes occurred more than 10 years before the start of the GPS observations. Because of their relatively smaller magnitudes, their postseismic deformation effect should also be limited. Thus the postseismic deformation signals are believed to be no more than 1 mm/yr and restricted to the epicentral areas, and would not affect our block motion estimation obtained mainly based on the far field deformation pattern.

4.1. South China Reference Frame

[14] The velocity solution we obtained from the analysis described above is with respect to the ITRF2000-NNR reference frame. For our kinematic analysis, we transfer the solution to a regional reference frame. We first compute a common angular velocity pole of 96 stations located in the south China block (defined as part of the Chinese continent east of the Longmenshan and Xiaojiang faults and south of the north China craton) relative to the ITRF2000-NNR reference frame. We then eliminate potential outliers from the 96 station velocities through an iteration procedure, each time removing a site with the largest postfit residual and redo the angular velocity estimation, until all the postfit residual velocities are within 2 mm/yr. In total 10 outliers are eliminated whose locations appear to be randomly distributed, and 86 stations (whose locations are shown in the inset map of Figure 1) are used to define the south China block. The angular velocity pole of rotation from ITRF2000-NNR to south China is located at 57.92°N 146.70°E, with a counterclockwise rotation rate of 0.22°/Myr. Using this angular velocity the GPS velocity field is converted to the south China reference frame as defined (Figure 2).

4.2. GPS Velocity Filtering and Block Motion Model

[15] Although the velocity field we have obtained is continuous and coherent over all (Figure 2), we identify and remove a few possible outliers in the data set. These velocity outliers could be caused by various sources, such as monument instability, accidents that occurred during surveys, coseismic displacements, and receiver/antenna type mismatch between survey epochs. For the last possibility of receiver/antenna type mismatch, we have modeled antenna phase center offsets for nonchoke ring antennas on a few Ashtech receiver units in the 1999 field survey (for details of the modeling and correction please see *Z.-K. Shen et al.* [2001]), but it cannot be ruled out that some residual errors still remain in the velocity estimates. Also, numerous $M > 5$ earthquakes occurred in the region during the observation time period, including a *M*6.4 event that occurred near the northwest end of the Chongxing-Tonghai fault (Figure 2). Coseismic deformation of these events could have affected our estimates of station velocities for the sites located in the epicentral regions.

[16] We detect and remove these outliers in two steps. First, we deleted half a dozen obvious outliers which are clearly at odds with the neighboring sites by visual inspection. Second, a rigorous procedure for outlier detection is performed which is based on the inherent assumption of rigid block motion employed in our study:

[17] 1. For a given block, use all the velocities of stations located in the block to estimate the block angular velocity by least squares regression. Evaluate the postfit residual χ^2_n, where n is the number of sites in the block.

[18] 2. Remove the site with the largest postfit residual and use the remaining station velocities to reestimate the block angular velocity. Evaluate the postfit residual χ^2_{n-1}.

[1]Auxiliary material is available at ftp://ftp.agu.org/apend/jb/2004JB003421.

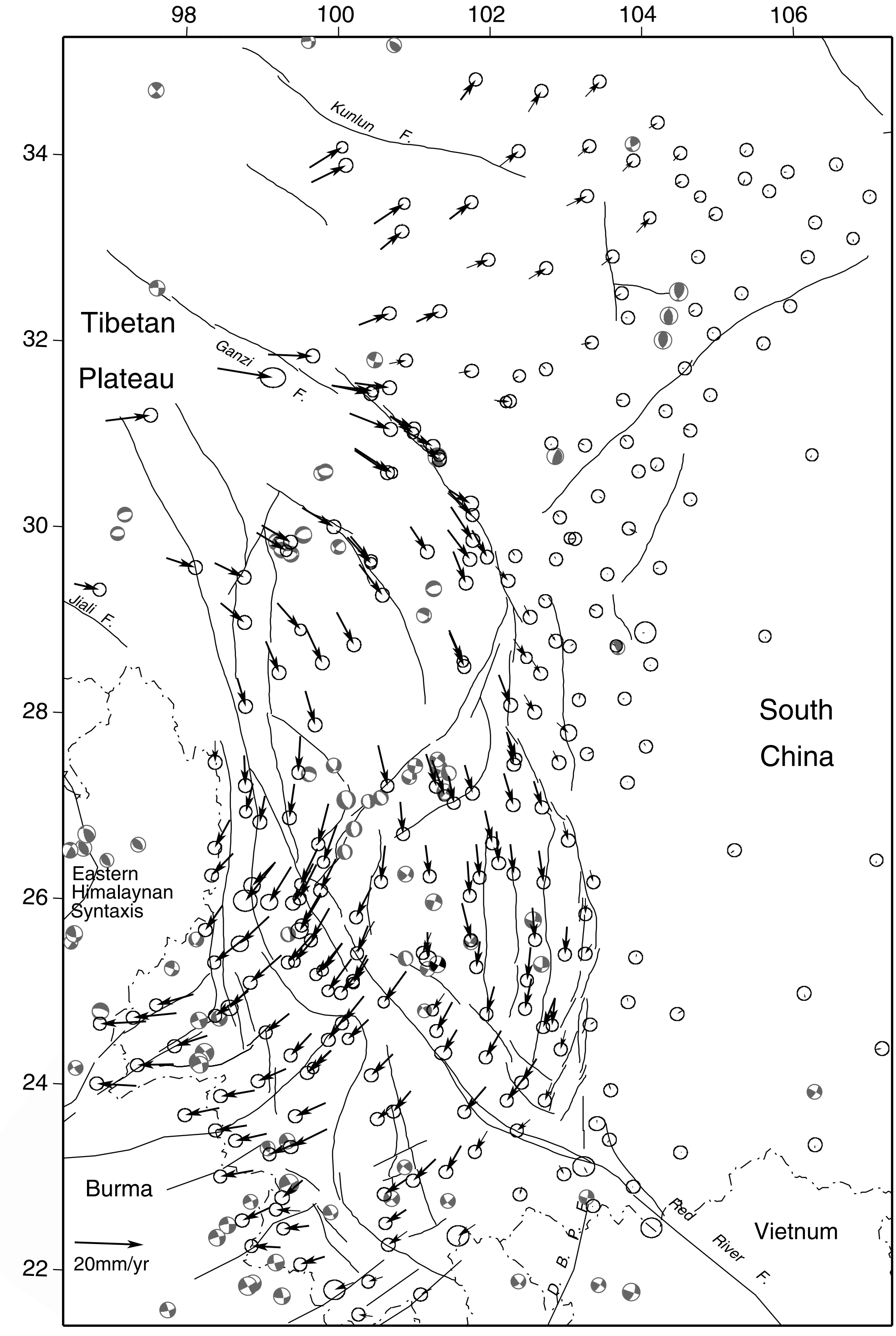

Figure 2. GPS velocity field with respect to the south China block. Each velocity arrow originates at the location of the site and points to its motion direction. The error ellipses represent 50% confidence. The earthquake focal mechanisms are from the Harvard CMT catalog, 1976–2003. The *M*6.4 earthquake that occurred 4 January 2000 at 25.3°N, 101.5°E is marked by black and white instead of gray and white focal mechanisms. Abbreviation is DBPF, Dien Bien Phu fault.

[19] 3. Use the F test to evaluate the significance of the outlier. The F value is defined as:

$$F = F\left(\chi_n^2, 2n-3; \chi_{n-1}^2, 2n-5\right) = \frac{\chi_n^2}{2n-3} \bigg/ \frac{\chi_{n-1}^2}{2n-5},$$

and the probability P(F) is evaluated. The site is removed if the F test exceeds 90% confidence, and the inspection process returns to step 1. The procedure is stopped when F test yields <90% confidence. Fifteen (about 6%) sites have been removed by this procedure, most of them are in the vicinity of block boundaries.

[20] A similar procedure to the above described outlier detection is performed to verify independence of neighboring blocks. In this procedure we first divide the study area into blocks separated by faults. Geologic and seismicity information is used for the initial definition of blocks, with the Xianshuihe-Anninghe-Xiaojiang, Lijiang, Red River, Longling, and Longmenshan faults as the initial block boundaries. Two significant GPS velocity gradient belts, which are associated with no known geologic faults, are also marked as block boundaries and will be described in detail later. We then use the *F* test to distinguish independent motions between adjacent blocks. Nonindependent blocks are merged together, until all relative block motions are independent at 90% confidence level. We should point out that our method is effective in identifying relative block motion at 90% confidence. However, if the *F* test result indicates less than 90% confidence this does not mean that there is absolutely no relative motion between the two potential blocks, but only that the GPS data do not require relative motion between the two blocks. In other words, relative block motion, if it exists, may be more subtle than what can be detected at a high (90% in this case) confidence level. Most of the blocks are verified to be rigid internally up to the limit of data precision (1–2 mm/yr), with only a couple of exceptions, which will be discussed later.

5. Results

[21] Figure 2 shows the velocity solution in the southeast borderland of the Tibetan Plateau with respect to the stable south China block. The first-order features of crustal deformation, clearly visible in Figure 2, are the left-slip motion along the Xianshuihe-Xiaojiang fault system and the prominent clockwise rotation around the EHS southwest of this fault zone. More detailed description and analysis of the block modeling and deformation along block boundaries are given in the following sections.

5.1. Block Motion

[22] On the basis of the deformation pattern shown in the GPS velocity field and inferred from other geologic [e.g., *Tang et al.*, 1993; *Wang and Burchfiel*, 1997, 2000; *Wang et al.*, 1998; *Xiang et al.*, 2000, 2002; *Zhang and Xie*, 2001; *Xu et al.*, 2003] and seismological [e.g., *Ma et al.*, 2000; *Zhang et al.*, 2001a; *Huang et al.*, 2002; *C.-Y. Wang et al.*, 2003; *Yang et al.*, 2003; *Division of Earthquake Monitoring and Prediction, State Seismological Bureau*, 1995; *Division of Earthquake Monitoring and Prediction*, China Seismological Bureau; 1999] studies, we divide the southeast borderland of the Tibetan Plateau into 5 major tectonic domains: the northern Sichuan region, the eastern Tibet region, the Sichuan-Yunnan fragment, the south China block, and the western Yunnan region (Figure 3). Some of the regions also deform internally and can be further divided into subblocks. For example, the northern Sichuan region is composed of the Longmenshan and Ahba subblocks based on GPS data which will be described later; the Sichuan-Yunnan fragment is composed of the Yajiang, Shangrila, and central Yunnan subblocks [*Wang and Burchfiel*, 2000; *Xiang et al.*, 2002; *Xu et al.*, 2003]; and the western Yunnan region is composed of the Baoshan and Lincang subblocks [*Wang and Burchfiel*, 1997; *Xiang et al.*, 2000] (Figure 3). We then derive the block motion parameters and obtain postfit residual χ^2 for each block or subblock. Our result shows that data from all of the blocks and subblocks fit the rigid block motion model well, as shown in Figure 3b, with their reduced postfit residual χ^2_ν below 1.0. We use the *F* test to determine independent blocks in a procedure described above. Eight independent blocks and subblocks in total are identified: south China, Ahba, Longmenshan, Yajiang, Shangrila, central Yunnan, Baoshan, and Lincang. The estimated block motion parameters and data fitting statistics are documented in Table 1. With respect to the Eurasia plate, the south China and Longmenshan blocks move east-southeastward at a rate of 7–8 mm/yr with small counterclockwise rotation; the Yajiang, Shangrila and central Yunnan blocks are rapidly moving southeast to south-southeastward (~13–18 mm/yr), with noticeable clockwise rotations (~0.9–1.9°/Myr); the Ahba block moves eastward at a rate of ~11 mm/yr and rotates clockwise at about 0.18°/Myr. Paleomagnetic studies show that a total of 4–17° clockwise rotation has occurred for the southern Sichuan-Yunnan fragment since the Paleocene-Eocene time [*Yoshioka et al.*, 2003; *Otofuji et al.*, 1998]. Assuming the rotation started with the formation of the Xianshuihe fault ~4 Ma [*Wang et al.*, 1998], the average rotation rate is ~1–4°/Myr. This estimate is in agreement with our results of ~1.4°/Myr and ~1.9°/Myr for the Yajiang and Shangrila blocks, respectively.

5.2. Sichuan-Yunnan Fragment

[23] The Sichuan-Yunnan fragment is regarded as a unique tectonic terrane, whose boundaries are usually defined as the Xianshuihe fault to the north, Anninghe-Zemuhe-Xiaojiang fault zone to the east, Lancang-Jinsha fault zone to the west, and Red River fault zone to the south [*Kan*, 1977; *Li and Wang*, 1977; *Wang et al.*, 1998]. The GPS velocity field relative to the Sichuan-Yunnan fragment is shown in Figure 4a, with velocity profiles across several fault strands revealed in Figure 5. To plot velocity profiles across a given fault or deformation zone, we first rotate the velocity field to establish a local reference frame with respect to a block on one side of the fault, such that there is no rotational effect left on this side of the velocity field. Fault slip rates are then estimated by taking far-field differences in velocity across chosen faults.

[24] We determine left-lateral slip across the western, central, and eastern sections of the Xianshuihe fault at rates of 10 ± 2, 10 ± 2, and 11 ± 2 mm/yr, respectively (Figure 4). There are no significant fault-normal motions across the fault (Figures 5a–5c). Our result is consistent with the 10 mm/yr left slip across the Xianshuihe fault reported by *Chen et al.* [2000]. We find 4 ± 2 mm/yr of left slip across both the Anninghe and Daliangshan faults, suggesting that the two faults define a ~50-km-wide subblock between them; however, more data would be needed to better resolve the partitioning of slip between the two subparallel faults (Figure 5d). Linking a right step between the Anninghe and Xiaojiang fault, the Zemuhe fault slips left laterally at a rate of 7 ± 2 mm/yr and extends at a rate of 3 ± 3 mm/yr across (Figure 5e). The Xiaojiang fault shows little fault-normal motion but a left slip of 7 ± 2 mm/yr (Figure 5f). Other mapped faults located west of and in parallel with the Xiaojiang fault, the Puduhe, Yimen, and

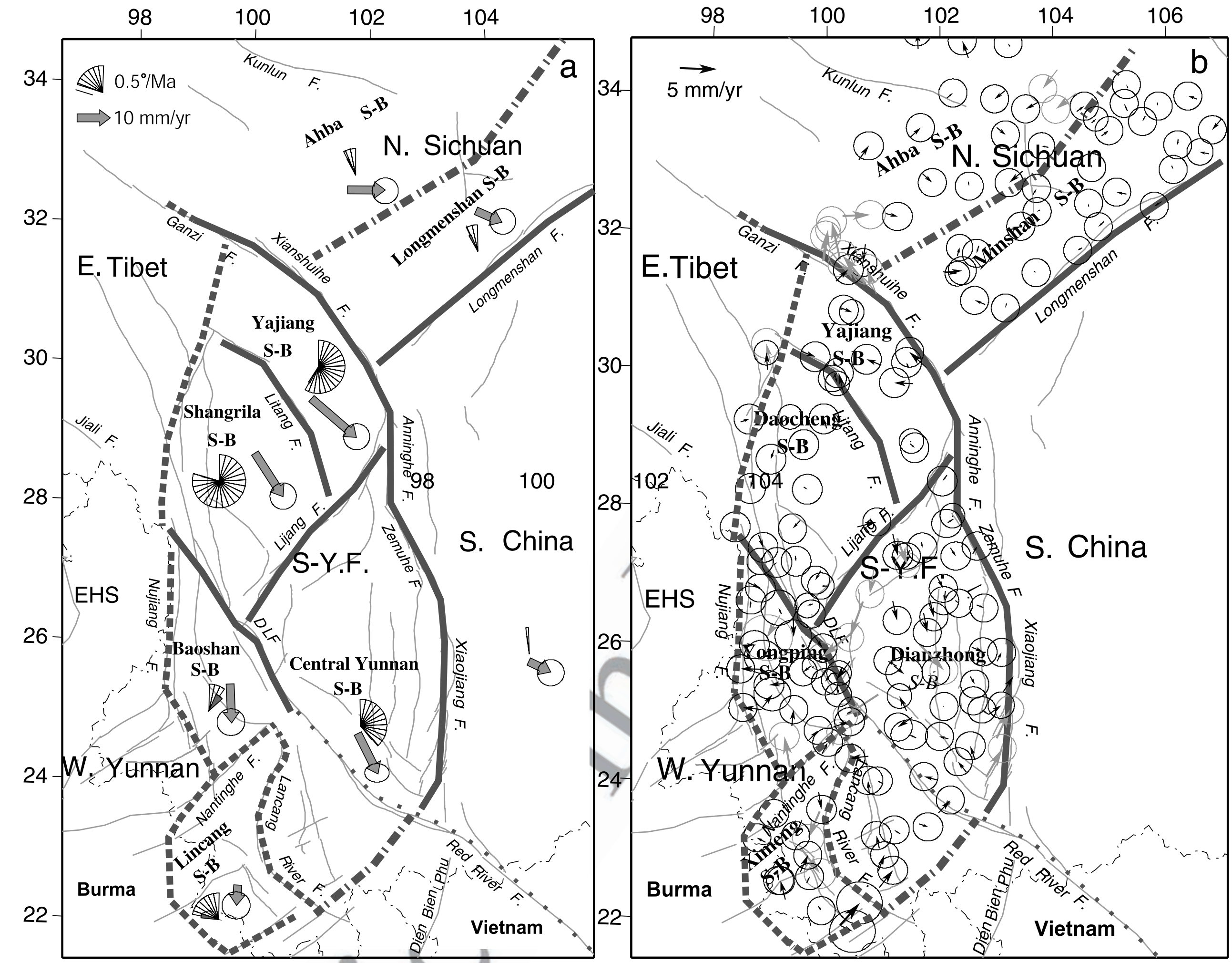

Figure 3. (a) Delineation of deformation blocks and their motions with respect to the Eurasia plate. Solid lines are the boundaries of crustal elements where velocity gradient can be well associated with known active faults, dashed lines are the ones with no precise known locations, dot-dashed lines are new boundaries required by GPS velocity data, and dotted line denotes a former block boundary which appears abandoned because of insignificant deformation found across. The fan-shaped symbols denote block rotation rates referenced to zero azimuth, with their uncertainties marked by fans with smaller radii. Arrows are the block velocities, with the error ellipses representing 95% confidence. The specific rates of block rotation and translation and angular velocities are listed in Table 1. (b) GPS velocity postfit residuals of the block motion model. Error ellipses represent 50% confidence. Gray arrows are outliers which are not used in block motion parameter evaluation. Abbreviations are EHS, eastern Himalayan Syntaxis; S-YF, Sichuan-Yunnan fragment; S-B, subblock.

t1.1 **Table 1.** Microblock Motion Result With Respect to the Eurasian Plate[a]

				Angular Velocity				Reference Point Location		Translation Rate, mm/yr		
t1.3	Microblock	Number of Sites	χ^2_ν	°/Myr	°N	°E	Corr	°N	°E	East	North	Rotation Rate, °/Myr
t1.4	South China block	86	0.247	0.083 ± 0.014	63.8 ± 1.6	181.8 ± 9.6	0.744	28.0	106.0	6.36 ± 1.65	−3.71 ± 1.61	0.04 ± 0.01
t1.5	Ahba subblock	15	0.712	0.209 ± 0.008	62.6 ± 23.5	103.9 ± 1.5	0.732	33.2	102.4	11.39 ± 1.61	−0.29 ± 1.59	0.18 ± 0.01
t1.6	Longmenshan subblock	28	0.292	0.183 ± 0.026	53.8 ± 10.4	122.6 ± 8.3	0.992	32.3	104.0	7.68 ± 1.58	−3.72 ± 1.58	0.17 ± 0.03
t1.7	Yajiang subblock	12	0.687	−1.409 ± 0.018	24.8 ± 1.0	96.2 ± 0.8	−0.961	29.5	101.5	13.72 ± 1.60	−11.43 ± 1.61	−1.40 ± 0.02
t1.8	Shangrila subblock	20	0.442	−1.911 ± 0.010	25.5 ± 0.2	95.7 ± 0.3	−0.852	28.4	99.8	8.69 ± 1.62	−12.98 ± 1.62	−1.91 ± 0.01
t1.9	Central Yunnan subblock	45	0.616	−0.925 ± 0.013	22.1 ± 0.3	95.0 ± 0.5	−0.868	24.5	102.0	5.450 ± 1.77	−11.49 ± 1.78	−0.93 ± 0.01
t1.10	Baoshan subblock	22	0.621	−0.253 ± 0.092	21.7 ± 5.2	72.7 ± 20.9	−0.990	25.0	99.5	0.645 ± 1.71	−11.72 ± 1.65	−0.23 ± 0.09
t1.11	Lincang subblock	10	0.701	0.525 ± 0.044	21.9 ± 1.0	106.2 ± 4.8	−0.833	22.5	99.5	−0.60 ± 1.73	−6.09 ± 1.67	0.52 ± 0.05

t1.12 [a]Parameters are χ^2_ν, reduced postfit chi-square; reference point location, location where translation and rotation are referenced.

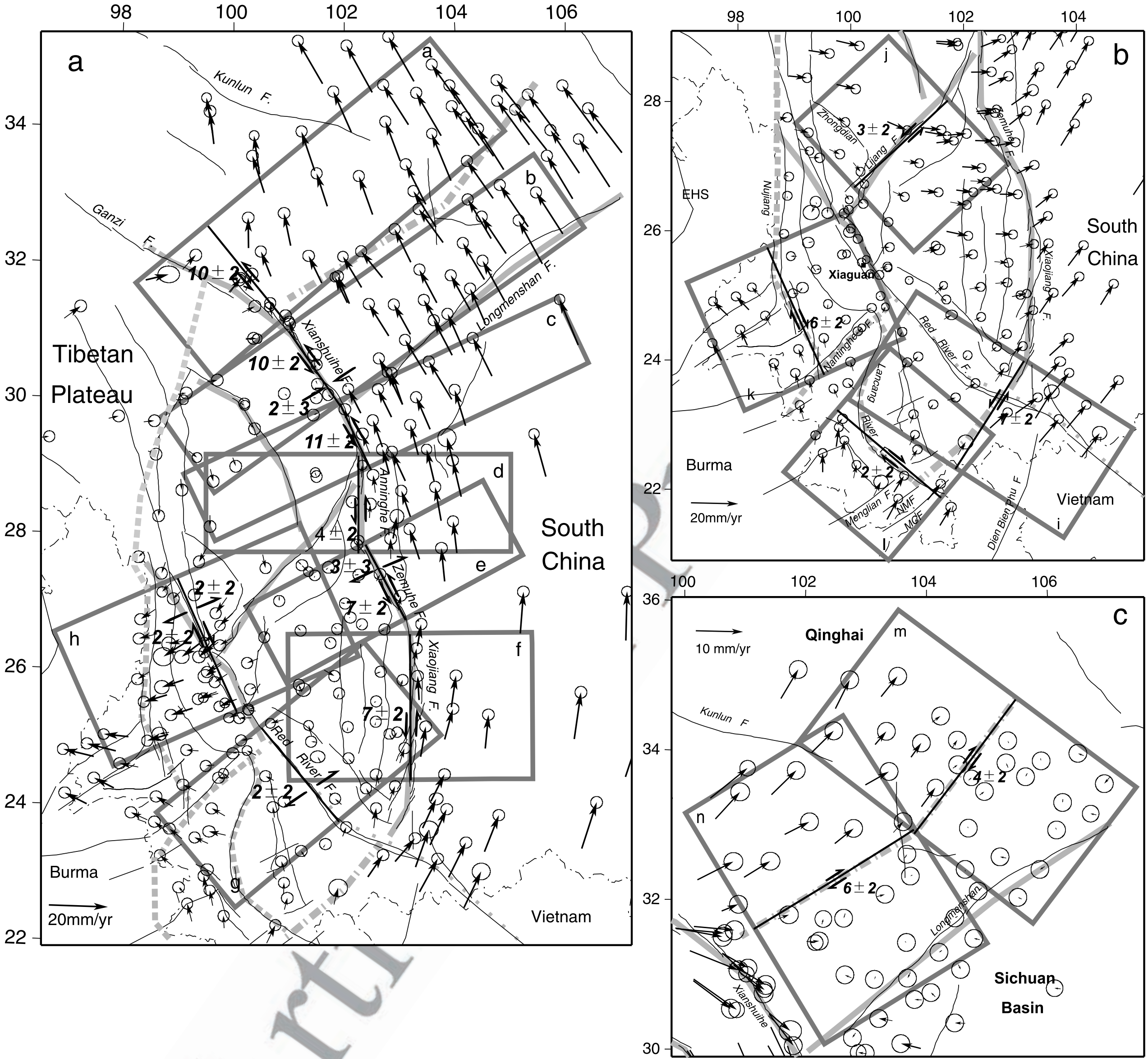

Figure 4. (a) GPS velocity field with respect to the Sichuan-Yunnan fragment, (b) close-up view of the Yunnan velocity field with respect to the Baoshan subblock, and (c) close-up view of the Northern Sichuan velocity field with respect to the Longmenshan subblock. The error ellipses represent 50% confidence. The thick straight lines along faults mark the strike directions, across which the fault slip rates are measured, and the results are given next to the slip vector pairs. The gray rectangular frames surrounding fault segments mark the regions within which stations are depicted for slip rate estimation, and their velocity profiles are shown in Figure 5.

Yuanmou faults (Figure 1), show no detectable motion across; therefore the left-lateral strike slip is confined within ~30 km of the Xiaojiang fault.

[25] Figures 5g–5h show deformation across the northwest section of the Red River fault within China. We divide this part of the Red River fault into two segments, the northwest and central segments separated at Midu at about 25°N (Figure 1). About 2 ± 2 mm/yr right slip and 2 ± 2 mm/yr extension are measured across the northwest segment. Another ~4 mm/yr NE-SW extension is detected across a deformation zone about 120 km northeast of this segment of the Red River fault (Figures 4 and 5h). This deformation pattern is associated with a complex fault system (including the Zhongdian, southern Lijang and Chuxiong-Tonghai faults), and the extension is possibly related to a cluster of pull-apart basins associated with the Red River fault system and deformation at corners of rotating fault-bounded blocks [*Wang et al.*, 1998; *Chen et al.*, 2000]. The right-slip rate across the central segment is about 1 ± 2 mm/yr (Figures 4 and 5g). This result is different from the Plio-Quaternary long-term slip rates of ~5 mm/yr [*Replumaz et al.*, 2001] and 2~7 mm/yr [*Allen et al.*, 1984] estimated from offsets of ~25 km over the past 5 Myr for the same segment of the fault. The low rates we find are consistent with the slip rate estimates of <2.7 mm/yr (averaged over thousands of years) inferred from a fault-

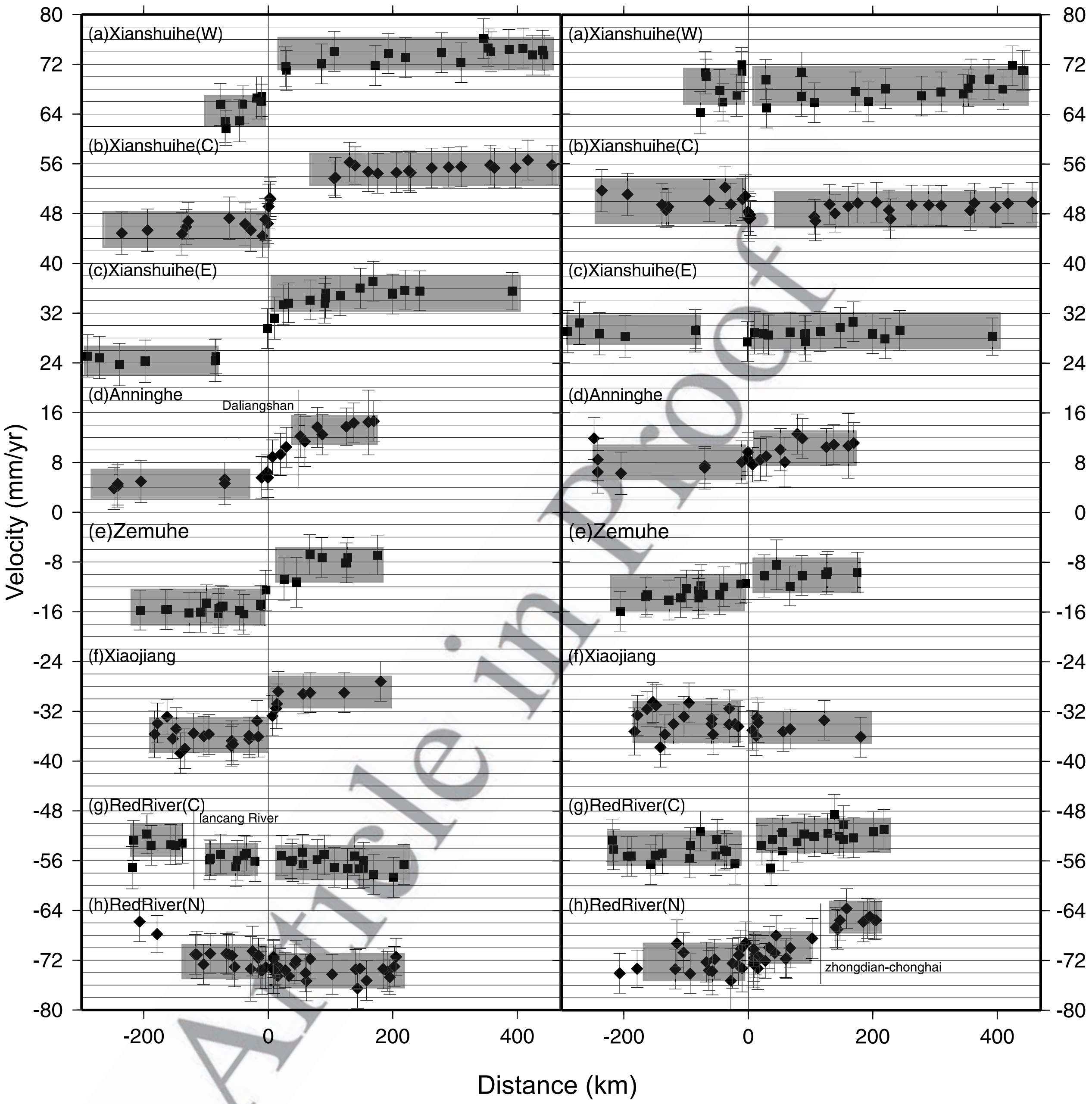

Figure 5. GPS velocity profiles across major active faults and areas. (left) Fault parallel (sinistral positive) and (right) fault-normal (extensional positive) components, with respect to the distance along profile. Data entries are indexed by regions outlined in Figures 4, 6, and 7. Data are shown with 2σ. The squares and diamonds are used alternatively to distinguish between adjacent entries. Vertical bars denote the locations of main faults; the added short bars in Figures 5d, 5g, and 5h denote the locations of the Daliangshan, Lancang River, and Zhongdian-Chenghai faults, respectively. Gray bars depict the scattering range of data on both sides of a fault. SEXF, southwest extension of the Xiaojiang fault.

trenching study [*Weldon et al.*, 1994], and 1∼2 mm/yr (averaged over a few years) derived using GPS along the southern segment of the fault within Vietnam [*Duong and Feigl*, 1999; *Feigl et al.*, 2003]. Thus the GPS results suggest that at present time the Red River fault does not appear to behave like a dominant intracontinental transform fault in the region as it used to. Other faults, such as the Litang and Longling faults, play a role at least as important as, and perhaps more important than the Red River fault in accommodating the regional crustal deformation.

[26] Assuming that the central segment of the Red River fault separates two subblocks located north and south of the fault, respectively, we use the *F* test to test independence of the two subblocks, and we obtain a confidence level of 84.7%. This result is less than the 90% confidence threshold we set for block independence, indicating that deformation

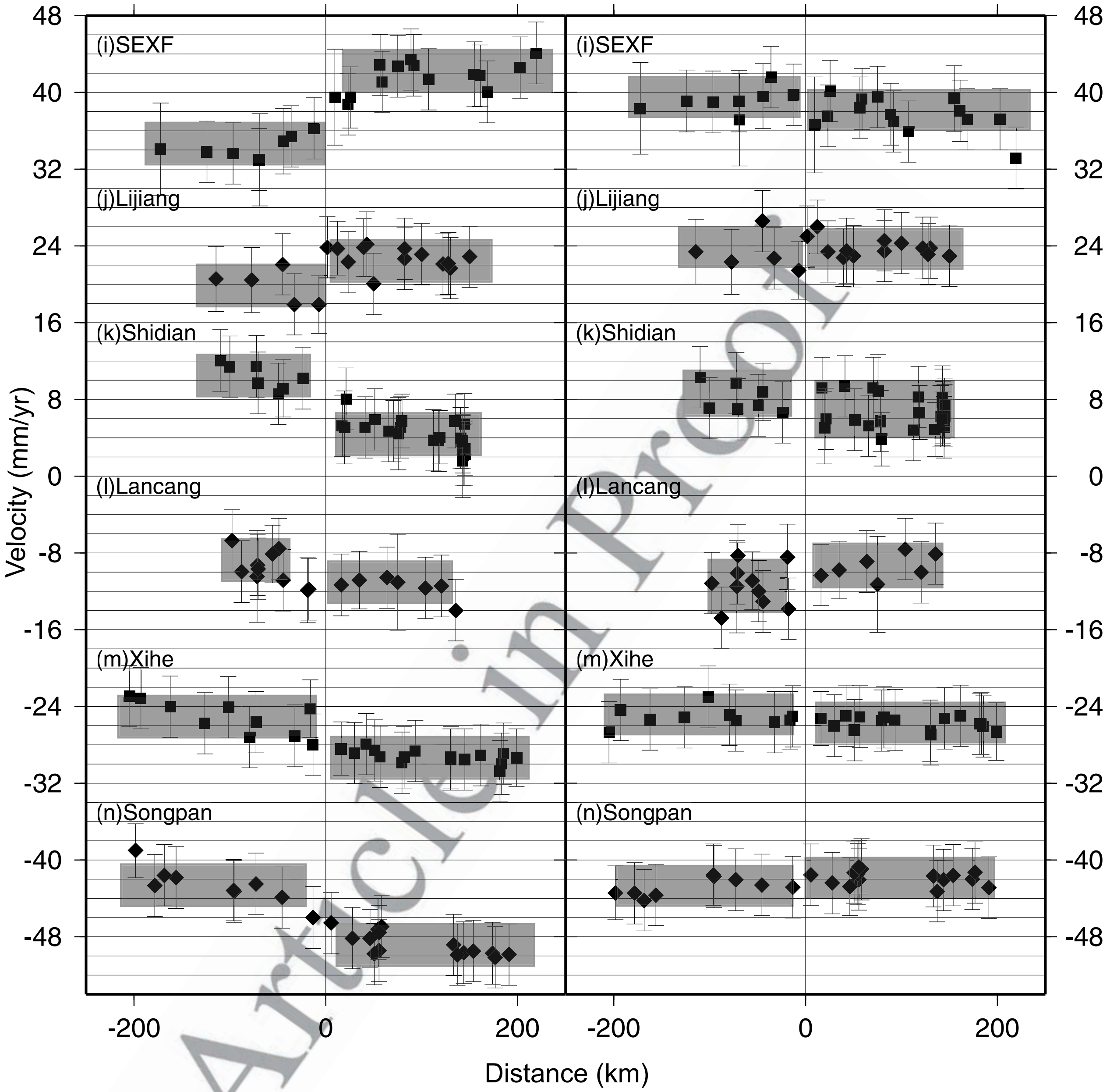

Figure 5. continued

across the fault is not very distinctive at the detection level of 1–2 mm/yr at present time. We therefore merge the two subblocks into a central Yunnan subblock (Figure 3). The east boundary of the subblock is the Xiaojiang fault in the north and its south-southwestward extension in the south, with the latter crosscutting the Red River fault system and slipping left laterally at a rate of 7 ± 2 mm/yr (Figures 4b and 5i).

[27] Our results show that the Sichuan-Yunnan fragment is not rigid internally, but deforms along some small-scale yet seismically active structures, such as the Lijiang, Zhongdian, Chonghai, and Litang faults (Figure 1). Along the Lijiang fault we infer ~3 mm/yr left slip (Figures 4b and 5j). This finding is supported by regional seismicity studies, as *Xiang et al.* [2000] reported an active seismic zone along this fault system. Moderate contemporary seismicity is found along the Litang fault, where our GPS network (particularly southwest of the fault) is too sparse to make a precise measurement of its slip rate. However, block motion analysis reveals that the Shangrila subblock located south of the fault rotates 1.9°/Myr clockwise with respect to the Eurasia reference frame, faster than the 1.4°/Myr clockwise rotation of the Yajiang subblock north of the fault. The relative motion between the two subblocks yields left lateral slip along the Litang fault at a rate of about 4 mm/yr.

5.3. Western Yunnan Region

[28] The western Yunnan region is defined as the area southwest of the Sichuan-Yunnan fragment. Two groups of faults dominate the regional tectonics: one is a fault zone continued SSE from the right-lateral Nujiang fault (here named the "Shidian deformation zone"), which is cut into

segments by another group of faults trending northeast represented by the Longling fault [*Wang and Burchfiel*, 1997; *Deng et al.*, 2003]. Relative to a regional GPS tracking site at Xiaguan (on the Baoshan subblock, Figure 4b), stations within the central Yunnan subblock are moving east to ENE, whereas stations west of the Shidian deformation zone are moving NW to NNW. The differential motion is ~7 mm/yr east-west extension across the Chenghai, Dali, and north segment of Red River faults (Figure 5h). There is also a ~6 mm/yr right-lateral shear across the Shidian deformation zone (Figures 5k and 4b). About 300 km west lies the Sagaing fault, which *Vigny et al.* [2003] found absorbs >20 mm/yr of the 35 mm/yr right lateral motion between India and Sundaland. The rest has to be distributed over a broad area on both sides of the Sagaing fault, and the right lateral shear in the Shidian region may be part of the deformation suggested by *Vigny et al.* [2003]. Crustal deformation in the region further south takes the form of east-west extension. Because of the sparse distribution of GPS sites in the region it is difficult to associate the deformation to specific faults. However, if it is attributed to the south segment of the Lancang River fault which is trending northwest, the deformation rate across the fault is 2 ± 2 mm/yr extension and 2 ± 2 mm/yr right slip (Figures 4b and 5l). Our results are consistent with that of *Holt et al.* [1995], who predicted east-west extension in south Yunnan based mainly on modeling seismic moment tensor data (the area includes both strike-slip and normal focal mechanisms, Figure 2). The near east-west extension also agrees with regional geology, which is evidenced by the presence of several small pull-apart basins in the area [*Wang et al.*, 1998].

5.4. Northern Sichuan Region

[29] The northern Sichuan region is defined as the area northwest of the Longmenshan fault and northeast of the Xianshuihe fault (Figure 3). The region is characterized by high mountain ranges such as the Longmen Shan, Min Shan, Qionglai Shan, Daxue Shan, and Bayankela Shan. A sharp topographic contrast exists across the southeast boundary of the region [*Kirby et al.*, 2000]. Such a geomorphic feature makes one wonder if active crust shortening is taking place across this zone. However, our GPS results indicate no obvious shortening (<3 mm/yr) across the Longmenshan fault (Figure 2), which is consistent with the findings of *King et al.* [1997] and *Chen et al.* [2000].

[30] Our GPS results detect a velocity gradient zone trending northeast (here named the "Songpan-Xihe deformation zone"), located ~150 km northwest of and parallel to the Longmenshan fault (Figure 2). The deformation zone seems to be quite broad, over a range of ~100 km in scale. Relative motion across the entire deformation zone is determined as right-lateral shear of 4–6 mm/yr with virtually zero normal motion across (Figures 4c and 5m–5n). Assuming rigid blocks on both sides of the deformation zone, we estimate angular velocities of the Longmenshan and Ahba blocks with respect to the Eurasia plate (Table 1). The small postfit residuals of the Longmenshan region indicate that its deformation is indeed block-like (Figure 3b). The deformation field in the Ahba region is moderately distributed, and 4 westernmost sites of the region are excluded to allow realization of a coherent Ahba block.

6. Discussion

6.1. Geometry and Kinematics of the Sichuan-Yunnan Fragment

[31] The Sichuan-Yunnan fragment plays an important role in Tibetan Plateau tectonics, since a significant part of the eastward extrusion of the plateau involves this block. Here the Tibetan Plateau crust is being broken into smaller microblocks, which are translated and rotated as this "block" is transported out of the plateau and turns gradually from moving eastward to southward along the way. Because of the unique role the Sichuan-Yunnan fragment has played in understanding Tibetan Plateau tectonics, its geometry and kinematic features are of special interests and have attracted attention of the tectonic research community.

[32] Along the northern boundary of the Sichuan-Yunnan fragment we find 10 ± 2 mm/yr left slip across both the northwest and central sections of the Xianshuihe fault, consistent with 9.6 ± 1.7 mm/yr and ~14 mm/yr Holocene slip across the same segments of the fault reported by *Li et al.* [1997] and *Xu et al.* [2003], respectively. Our result also agrees with *Allen et al.*'s [1991] estimate of 15 ± 5 mm/yr Holocene slip rate. *Wen et al.* [1996] derived a Holocene slip rate of 7.2 mm/yr along the central segment of the fault, which is slightly smaller than our GPS result. Average slip for the past 2–4 Myr was estimated as 15–30 mm/yr based on offset of ~60 km by *Wang et al.* [1998], but the uncertainty of this rate is much greater than that of the Holocene slip estimates. The good agreement between the geodetic and Holocene geological results suggests steady deformation rates of the fault at present time.

[33] The Xianshuihe fault joins the Anninghe-Zemuhe fault system at its south end (Figure 1). *Xu et al.* [2003] found 6.5 ± 1 and 6.4 ± 0.6 mm/yr Holocene left slip rates across the Anninghe and Zemuhe faults from field geology, respectively. *Ren* [1990] reported a Holocene slip rate of 4.9 mm/yr along the Zemuhe fault. These results are a bit greater than the ~4 mm/yr left slip we infer across the Anninghe fault, but less than the total of ~8 mm/yr left slip the GPS data indicate across the Anninghe and Daliangshan faults. Such a discrepancy may suggest temporal variation of slip partitioning between the Anninghe and Daliangshan faults: with the Anninghe fault currently slipping somewhat slower and the Daliangshan fault a bit faster than their geological averages. Further field work, particularly on the Daliangshan fault, is needed to test this hypothesis. A pull-apart basin is located at a left step between the Anninghe and Zemuhe faults and extends in the NNE direction [*Zhang and Xie*, 2001]. Our result shows 3 ± 3 mm/yr ENE extension across the Zemuhe fault and the pull-apart basin associated with it. The strike slip motion along the Anninghe-Zemuhe fault system and the opening of the pull-apart basin result from the southward motion of the Sichuan-Yunnan fragment relative to the south China block.

[34] GPS studies [*King et al.*, 1997; *Chen et al.*, 2000; this study] indicate that the central segment of the Red River fault does not show significant deformation (<2 mm/yr) at present time. The southern segment of the Red River fault in

Vietnam, although long considered to be the block boundary between Indochina and south China, was also found to slip at low rates (1–2 mm/yr) by GPS [*Duong and Feigl*, 1999; *Feigl et al.*, 2003]. This is consistent with a far field GPS study in the region [*Michel et al.*, 2000], which showed no significant deformation across this segment of the fault. Geologic studies of offset Holocene and Pliocene features placed 1–5 mm/yr right slip along the central and southern segment of the fault [*Allen et al.*, 1984; *Wang et al.*, 1998; *Replumaz et al.*, 2001]. In addition, seismicity has been weak along this fault for the past 30 years. On the basis of these observations, it can be concluded that the central and southern segments of the Red River fault do not deform at a high rate at present time. On the other hand, about 200 km southwest of the fault and in the neighborhood of the south segment of the Lancang River fault, ~2 mm/yr right slip is detected across a zone trending northwest. Therefore the south section of the Lancang River fault, or a deformation zone associated with the fault system seems to be the southern boundary of the Sichuan-Yunnan fragment, at least at the present time (Figures 3 and 4).

[35] The GPS velocities indicate that the left-lateral strike-slip motion along the Xiaojiang fault system extends southwestward across the Red River fault (Figures 2, 4b, and 5j). Geological investigations showed that the Red River fault system is bent, but not cut, by the left-lateral shear of the Xianshuihe-Xiaojiang fault system, resulting in minor oblique slip along the Red River fault [*Wang et al.*, 1998]. It has been suggested that the Dien Bien Phu fault takes up a major part of the transferred left-lateral motion, and the Xianshuihe-Xiaojiang-Dien Bien Phu fault system forms the east boundary of the crustal material that has rotated clockwise relative to the south China block during late Cenozoic time [*Wang et al.*, 1998; *Michel et al.*, 2000]. By contrast, *Lacassin et al.* [1998] inferred from long-term river offsets that the left-lateral shear deformation is distributed broadly on several left-slip faults northwest of the Dien Bien Phu fault, such as the Nam Ma, Mengxing, and Mae Chan faults, at a cumulative rate of 1.9–7.5 mm/yr. Our GPS observations are more consistent with those of *Lacassin et al.* [1998] (Figures 1 and 2), although we cannot precisely correlate the deformation with known faults in the region yet. There appears to be a gap of mapped faults in the region immediately south of the central segment of the Red River fault and north of the Nam Ma, Menxing, and Mae Chan faults. This area is in the high mountains close to the Sino-Vietnam border, and future field mapping will be important to locate corresponding faults. Nevertheless, GPS observations and geological investigations attest that the northernmost part of Indochina is not a rigid block separated from the south China block by the Red River fault. Instead, it inherits a significant part of the left-slip motion southwestward from the Xiaojiang fault separating the Sichuan-Yunnan fragment from the south China block. Deformation seems to become diffuse south of the southern segment of the Lancang River fault.

[36] About 2 mm/yr right slip and 2 mm/yr near east-west extension are detected across the northwest segment of the Red River fault which is considered the southwest boundary of the Sichuan-Yunnan fragment (Figures 4a and 5h). No precise determination of the northwest boundary for the Sichuan-Yunnan fragment can be inferred from this study, due to sparse distribution of the GPS stations in the region west of the Shangrila subblock, where several faults such as the Red River, Lancang River, and Nujiang faults trend north-south and run parallel within a ~30-km-wide zone (Figure 1).

6.2. Deformation Around Northern Sichuan

[37] Despite of the striking geomorphic features of the Longmen Shan, the low shortening rate at present time (<1–3 mm/yr) [*King et al.*, 1997; *Chen et al.*, 2000; this study] and the lack of a Cenozoic foredeep [*Kirby et al.*, 2000], indicate limited Cenozoic shortening across this mountain belt. In contrast, a remarkable right-lateral shear zone trending northeast, the Songpan-Xihe deformation zone, is found ~150 km northwest of the Longmenshan fault between the Longmenshan and Ahba blocks (Figure 4c). This discovery is somewhat puzzling because the deformation cannot be correlated with a known active fault. Along the southwest section of the Songpan-Xihe deformation zone, a couple of short fault segments trending northeast have been mentioned in previous studies [*Ma*, 1989; *Tang et al.*, 1995]. Although no precise location was given, *Burchfiel* [2004], on the basis of GPS observations in the region, inferred existence of a northeast trending boundary west of the Longmen Shan with 8–15 mm/yr active right shear. However, geological documentation of contemporary faulting is rather limited, because of difficult accessibility, heavy vegetation, and lack of late Quaternary deposits in the region [*Deng et al.*, 1994]. Regional earthquakes of the past 30 years show a scattered seismicity pattern, nevertheless seismic events seem to align in a northeast direction around the northeast segment of this deformation zone (Figure 1). Further investigation is needed to better understand the tectonic deformation of the region.

[38] The eastward extrusion of Tibet has produced a right-lateral strike-slip boundary northwest and a left-lateral strike-slip boundary southwest of the Longmenshan block, and the Longmenshan block stays almost stationary with respect to the south China block. Thus the eastward motion of Tibet seems to be partitioned between a northern and a southern zone of extrusion. Extrusion of the northern plateau is accommodated mainly along the Qilian Shan-Nan Shan transpressional fault belt [*Chen et al.*, 2000; *Z.-K. Shen et al.*, 2001]), while extrusion of southern Tibet is rotated around the EHS in a complex, broadly deformed region and eventually absorbed in northern Indochina.

6.3. Deformation Dynamics

[39] Many dynamic models have been proposed to simulate the continental collision process between India and Asia and explain the mechanical evolution of Tibet that resulted from the collision. The most prominent ones can usually be categorized into two end-member models, as we described in the introduction section of the paper. One school of models prescribes the crust as being fractured into a limited number of tectonic blocks by large-scale strike-slip faults (hereafter called "block motion" model, e.g., *Tapponnier et al.*, 1982; *Peltzer and Tapponnier*, 1988; *Avouac and Tapponnier*, 1993; *Replumaz and Tapponnier*, 2003), whereas the other class of models treats the crust as a thin viscous sheet, whose deformation is broadly distributed (hereafter called "viscous sheet" model [e.g., *England and*

Molnar, 1997b; *Flesch et al.*, 2001]). A variation of the viscous sheet model was developed by *Royden et al.* [1997] and *F. Shen et al.* [2001], in which a layered viscous lithosphere is considered, whose viscosity has varied progressively during the development of the plateau, and viscous channel flow in the lower crust developed at its later stage (hereafter called ''channel flow'' model). Despite of their fundamental differences, all of these models acknowledge that the brittle upper crust likely deforms by discrete faulting. They differ dramatically with regards to the material properties and deformation style of the lower crust and uppermost mantle, which ought to be reflected at some scale in the deformation pattern at the Earth's surface. We attempt to compare first-order deformation patterns predicted by the different end-member models with the GPS observations.

6.3.1. Clockwise Rotation Around EHS

[40] GPS results show significant clockwise rotation in a region between the EHS and the left-lateral strike-slip Xianshuihe-Xiaojiang fault system. With respect to the south China block, this region changes its motion direction from east-southeastward south of the Ganzi-Xianshuihe fault to southward west of the Xiaojiang fault, and even to westward east of the Sagaing fault. Such a rotation pattern can also be identified in the instantaneous block motion rates from north to south (Table 1 and Figure 3b). All the models mentioned above involve clockwise rotation in the region, but the amounts vary. With respect to the south China block, the block motion and viscous sheet models usually predict southeast directed motion [e.g., *Flesch et al.*, 2001; *Replumaz and Tapponnier*, 2003] while the channel flow model suggests south directed rotation [*F. Shen et al.*, 2001].

6.3.2. Extent of Clockwise Rotation

[41] Our GPS result shows a quite limited extent of clockwise rotation for the region, for which the deformation models offered quite different predictions. The block motion models usually yield large-scale clockwise rotation for the region east of the Xiaojiang fault, sometimes covering the entire south China block. On the contrary, the viscous sheet and channel flow models predict clockwise rotation only within the southeast borderland of the Tibetan Plateau, and the channel flow model even predicts slightly counterclockwise rotation east of the Xiaojiang fault.

6.3.3. Eastward Motion of South China Block

[42] We estimate 7–8 mm/yr ESE motion of the south China block with respect to the Eurasian plate, a result consistent with the observations of *Shen et al.* [2000] and *Wang et al.* [2001]. This rate is only about 1/5 of the convergence rate between India and Asia, and is approximately in agreement with the predictions of the viscous sheet models but significantly less than that of block motion models (e.g., a rate of ~18 mm/yr for the last 5 Myr given by *Replumaz and Tapponnier* [2003]).

6.3.4. Regional Pattern of Deformation

[43] We find that although the Xianshuihe-Xiaojiang is the most dominant fault system in the region, deformation is not limited to this fault system, but distributed across numerous active faults such as the Lijiang, Litang, and northern segment of the Red River faults. At 1–2 mm/yr accuracy level we have identified seven coherent blocks without significant internal deformation (Figure 3a and Table 1). As the size of tectonic blocks bounded by crustal faults decreases, it becomes more difficult to consider the deformation as that of a few major tectonic blocks as proposed by the block motion model. There is still ''block tectonics'' but the scale and kinematics make this more consistent with a distributed deformation pattern. Thus, while large coherent blocks may dominate the continental deformation elsewhere in the collision zone (W. Thatcher, submitted to *Science*, 2005), deformation in the southeast borderland is broadly distributed over a wide region.

[44] Also, the lack of both active convergence in our GPS data and of significant Cenozoic contraction across the dramatic topographic escarpment of the Longmen Shan suggests that the eastern Tibetan Plateau thickened without significant crustal shortening. This suggests that lower crustal flow may have significantly contributed to the morphology of the eastern plateau. Ultimately, resolving vertical motions at submillimeters per year resolution would be valuable to constrain the 3D expression of the deformation in the region.

6.3.5. Deformation Around Southwest Yunnan

[45] On a regional scale, we find that no model agrees well with the deformation field around southwest Yunnan, where our GPS result demonstrates southwestward motion with respect to the south China block. The channel flow model [*F. Shen et al.*, 2001] comes closest, predicting southward instead of the observed southwestward motion with respect to south China. Such a discrepancy between the channel flow model prediction and the data may result from the model missing the effect of eastward subduction of the Indian plate beneath Sundaland and westward back-arc spreading associated with the subduction process [*Paul et al.*, 2001].

6.3.6. Summary

[46] We find that although none of the models is in complete agreement with the GPS observations, the viscous sheet models, particularly the ones with the channel flow effect in the lower crust incorporated, seem to do a better job overall. It should be pointed out that block motion models may explain the early phase of the Indo-Asian collision process better; at that time Tibetan crust was not thickened enough to allow viscous channel flow to be developed in the lower crust, and lateral extrusion perhaps played a greater role in accommodating India indentation into the Asian continent. At present time, however, the effect of viscous flow in the lower crust of Tibet appears to be playing an important role in crustal deformation of the southeast borderland of the Tibetan Plateau. This view is also supported by seismic tomography studies, which showed widely developed low-velocity zones in the lower crust of the region west of the Longmenshan and Xiaojiang faults and north of the Red River fault [*C.-Y. Wang et al.*, 2003; *Huang et al.*, 2002; *Liu et al.*, 2005]. The Red River fault, despite of being perhaps a mechanically weak zone in the lithosphere, is no longer tectonically active as before, probably because its location and geometry make it less efficient to transfer crustal material out of Tibet. The relatively small sizes of the microblocks and their rotation pattern demonstrated in our GPS results seem to suggest a model with a mechanically weak lower crust experiencing distributed deformation underlying a stronger upper crust.

Such a model still waits to be verified further, since we have no direct or indirect measurements of the deformation and rheology of the lower crust in this region. However, if the model is correct, it suggests that deformation of the southeast borderland is driven mainly by eastward motion of the plateau and gravitational buoyancy forces. Crustal flow gets narrower north of the EHS due to the EHS north-northeastward advancement [*Xu and Kamp*, 2000]. Further east, the crustal flow turns gradually from eastward to southward motion because of the blocking in the east by the rigid and slow moving south China block. Further south, the flow pattern spreads out possibly due to the influence of India's eastward subduction underneath Sundaland, and by the gravitational buoyancy force associated with the sharp topographic gradient across the region: the mean elevation drops from ~5 km in northern Sichuan-Yunnan fragment to merely ~1 km in northern Indochina within ~500 km.

[47] **Acknowledgments.** We are very grateful to Zongjin Ma, Zhijun Niu, Xinlian Chen, Xi'an Lai, and Jianzhong Sun for their critical roles in creating the Crustal Motion Observation Network of China and making data available to this study. Field observations organized by Zusheng Zhang, Liren Huang, Qi Wang, and Xinzhao You are especially acknowledged. The authors thank Peizhen Zhang, An Yin, Dave Jackson, Jin Ma, Xiwen Xu, Xueze Wen, Erqi Wang, and Weijun Gan for helpful discussions. Reviews and comments by Peter Molnar, Bob King, Jeff Freymueller, Clark Burchfiel, and Gilles Peltzer helped improve the manuscript greatly. Critical editing and comments by Isabelle Manighetti are also acknowledged. We thank Danan Dong for the discussions of using his QOCA software, Yehuda Bock and Peng Fang for making SOPAC's global solutions available, and Hanrong Sun for allowing us to use the computing facilities at the GPS data Center, CEA for this study. Graphic works are partially done using the GMT software. This work is supported by grants from the Chinese Ministry of Science and Technology 2002CCA04500, 2001CCB01100, and 2004CB418403.

References

Allen, C. R., A. R. Gillespie, Y. Han, K. E. Sieh, B. Zhang, and C. Zhu (1984), Red River and associated faults, Yunnan province, China: Quaternary geology, slip rate and Seismic hazard, *Geol. Soc. Am. Bull.*, *95*, 686–700.

Allen, C. R., Z. Luo, H. Qian, X. Wen, H. Zhou, and W. Huang (1991), Field study of a highly active fault zone: The Xianshuihe fault of southwestern China, *Geol. Soc. Am. Bull.*, *103*, 1178–1199.

Altamimi, Z., P. Sillard, and P. Boucher (2002), ITRF2000: A new release of the international Terrestrial Reference Frame for earth science applications, *J. Geophys. Res.*, *107*(B10), 2214, doi:10.1029/2001JB000561.

Avouac, J. P., and P. Tapponnier (1993), Kinematic model of active deformation in central Asia, *Geophys. Res. Lett.*, *20*, 895–898.

Bilham, R., K. Larson, J. Freymueller, and Project Idylhim (1997), GPS measurements of present-day convergence across the Nepal Himalaya, *Nature*, *386*, 61–64.

Briais, A., P. Patriat, and P. Tapponnier (1993), Updated interpretation of magnetic anomalies and seafloor spreading stages in the South China Sea: Implications for the Tertiary tectonics of Southeast Asia, *J. Geophys. Res.*, *98*, 6299–6328.

Burchfiel, B. C. (2004), New technology; New geological challenges, *GSA Today*, *14*(2), 4–9.

Burchfiel, B. C., and E. Wang (2003), Northwest-trending, middle Cenozoic, left-lateral faults in southern Yunnan, China, and their tectonic significance, *J. Struct. Geology*, *25*, 781–792.

Burchfiel, B. C., Z. Chen, Y. Liu, and L. H. Royden (1995), Tectonics of the Longmen Shan and adjacent regions, *Int. Geol. Rev.*, *37*, 661–735.

Chen, S., C. Wilson, Q. Deng, X. Zhao, and Z. Luo (1994), Active faulting and block movement associated with large earthquakes in the Min Shan and Longmen mountains, northeastern Tibetan Plateau, *J. Geophys. Res.*, *99*, 24,025–24,038.

Chen, Q., J. Freymueller, Q. Wang, Z. Yang, C. Xu, and J. Liu (2004), A deforming block model for the present-day tectonics of Tibet, *J. Geophys. Res.*, *109*(B1), B01403, doi:10.1029/2002JB002151.

Chen, Z., B. C. Burchfiel, Y. Liu, R. W. King, L. H. Royden, W. Tang, E. Wang, J. Zhao, and X. Zhang (2000), Global Positioning System measurements from eastern Tibet and their implications for India/Eurasia intercontinental deformation, *J. Geophys. Res.*, *105*, 16,215–16,227.

Deng, Q., S. Chen, and X. Zhao (1994), Tectonics, seismicity and dynamics of Longmenshan Mountains and its adjacent regions, *Seismol. Geol.*, *16*, 389–403.

Deng, Q., P. Zhang, and Y. Ran (2003), Basic characteristics of active tectonics of China, *Sci. China, Ser. D*, *46*, 356–372.

Division of Earthquake Monitoring and Prediction, State Seismologic Bureau (1995), *Catalog of Chinese Historical Strong Earthquakes (2300 BC–1911)*, 514 pp., China Seismol. Press, Beijing.

Division of Earthquake Monitoring and Prediction, China Seismologic Bureau (1999), *Catalog of Chinese historical strong earthquakes (1912–1990 $M_s \geq 4.7$)*, 637 pp., China Seismol. Press, Beijing.

Duong, C., and K. L. Feigl (1999), Geodetic measurement of horizontal strain across the Red River fault near Thac Ba, Vietnam, 1963–1994, *J. Geod.*, *73*, 298–310.

England, P., and D. P. McKenzie (1982), A thin viscous sheet model for continental deformation, *Geophys. J. R. Astron. Soc.*, *70*, 295–321.

England, P. C., and P. Molnar (1997a), The field of crustal velocity in Asia calculated from Quaternary rates of slip on faults, *Geophys. J. Int.*, *130*, 551–582.

England, P. C., and P. Molnar (1997b), Active deformation of Asia: From kinematics to dynamics, *Science*, *278*, 647–650.

Feigl, K. L., C. Duong, M. Becker, D. Tran, K. Neumann, and X. Nguyen (2003), Insignificant horizontal strain across the Red River fault near Thac Ba, Vietnam from GPS measurements 1994–2000, *Geophys. Res. Abstr.*, *5*, Abstract 04707.

Flesch, L. M., W. E. Holt, and A. J. Haines (2001), Dynamics of the India-Eurasia collision zone, *J. Geophys. Res.*, *106*, 16,435–16,460.

Gilley, L. D., T. M. Harrison, P. H. Leloup, F. J. Ryerson, O. M. Lovera, and J.–H. Wang (2003), Direct dating of left-lateral deformation along the Red River shear zone, China and Vietnam, *J. Geophys. Res.*, *108*(B2), 2127, doi:10.1029/2001JB001726.

Harrison, T. M., W. J. Chen, P. H. Leloup, F. J. Ryerson, and P. Tapponnier (1992), An early Miocene transition in deformation regime within the Ailao Shan-Red River shear zone, Yunnan, and its significance for Indo-Asian tectonics, *J. Geophys. Res.*, *97*, 7159–7182.

Harrison, T. M., P. H. Leloup, F. J. Ryerson, P. Tapponnier, R. Lacassin, and W. Chen (1996), Diachronous initiation of transtension along the Ailao Shan–Red River shear zone, Yunnan and Vietnam, in *The Tectonic Evolution of Asia*, edited by A. Yin and M. T. Harrison, pp. 208–226, Cambridge Univ. Press, New York.

Herring, T. A. (2002), GLOBK: Global Kalman filter VLBI and GPS analysis program, version 10.0, Mass. Inst. of Technol., Cambridge.

Holt, W. E., M. Li, and A. J. Haines (1995), Earthquake strain rates and instantaneous relative motions within central and eastern Asia, *Geophys. J. Int.*, *122*, 569–593.

Holt, W. E., N. Chamot-Rooke, X. Le Pichon, A. J. Haines, B. Shen-Tu, and J. Ren (2000), Velocity field in Asia inferred from Quaternary fault slip rates and Global Positioning System observations, *J. Geophys. Res.*, *105*, 19,185–19,209.

Houseman, G., and P. England (1986), Finite strain calculations of continental deformation 1. Method and general results for convergent zones, *J. Geophys. Res.*, *91*, 3651–3663.

Houseman, G., and P. England (1993), Crustal thickening versus lateral expulsion in the Indian-Asian continental collision, *J. Geophys. Res.*, *98*, 12,233–12,249.

Houseman, G., and P. England (1996), A lithospheric thickening model for the Indo-Asian collision, in *The Tectonic Evolution of Asia*, edited by A. Yin and T. M. Harrison, pp. 3–17, Cambridge Univ. Press, New York.

Huang, J., D. Zhao, and S. Zheng (2002), Lithospheric structure and its relationship to seismic and volcanic activity in southwest China, *J. Geophys. Res.*, *107*(B10), 2255, doi:10.1029/2000JB000137.

Institute of Geology, China Seismological Bureau, and Seismological Bureau of Yunnan Province (1990), *The Active Faults of Southwest Region of Yunnan Province* (in Chinese), Seismological Pub. House, Beijing.

Kan, R. (1977), Study on the current tectonic stress field and the characteristics of current tectonic activity in southwest China (in Chinese), *Chin. J. Geophys.*, *20*(2), 96–107.

King, R. W., and Y. Bock (2000), Documentation for the GAMIT GPS analysis software, release 10.0, Mass. Inst. of Technol., Cambridge.

King, R. W., F. Shen, B. C. Burchfiel, L. H. Royden, E. Wang, Z. Chen, Y. Liu, X.-Y. Zhang, J.-X. Zhao, and Y. Li (1997), Geodetic measurement of crustal motion in southwest China, *Geology*, *25*, 179–182.

Kirby, E., K. X. Whipple, B. C. Burchfiel, W. Tang, G. Berger, Z. Sun, and Z. Chen (2000), Neotectonics of the Min Shan, China: Implications for mechanisms driving Quaternary deformation along the eastern margin of the Tibetan Plateau, *Geol. Soc. Am. Bull.*, *112*, 375–393.

Kong, X., and P. Bird (1996), Neotectonics of Asia: thin-shell finite element models with faults, in *The Tectonic Evolution of Asia*, edited by A. Yin and T. M. Harrison, pp. 18–34, Cambridge Univ. Press, New York.

Lacassin, R., A. Replumaz, and P. H. Leloup (1998), Hairpin river loops and slip-sense inversion on southeast Asian strike-slip faults, *Geology*, *26*, 703–706.

Larson, K. M., R. Burgmann, R. Bilham, and J. T. Freymueller (1999), Kinematics of the India-Eurasia collision zone from GPS measurements, *J. Geophys. Res.*, *104*, 1077–1093.

Le Dain, A. Y., P. Tapponnier, and P. Molnar (1984), Active faults and tectonics of Burma and surrounding regions, *J. Geophys. Res.*, *89*, 453–472.

Leloup, P. H., R. Lacassin, P. Tapponnier, U. Schärer, D. L. Zhong, X. H. Liu, L. S. Zhang, S. C. Ji, and T. T. Phan (1995), The Ailao Shan-Red River shear zone (Yunnan, China), Tertiary transform boundary of Indochina, *Tectonophysics*, *251*, 3–84.

Leloup, P. H., N. Arnaud, R. Lacassin, J. R. Kienast, T. M. Harrison, T. T. Phan, A. Replumaz, and P. Tapponnier (2001), New constraints on the structure, thermochronology, and timing of the Ailao Shan-Red River shear zone, SE Asia, *J. Geophys. Res.*, *106*, 6683–6732.

Li, P., and L. Wang (1977), Research on basic seismogeological characteristics in Yunnan and west Sichuan region, in *Discussion on Seismogeology and Seismic Intensity Zoning in Southwest China* (in Chinese), Seismol. Press, Beijing.

Li, T., Q. Du, and Z. You (1997), *The Active Xianshuihe Fault Zone and Seismic Risk Assessment* (in Chinese), Cartogr. Publ. House of Chengdu, Chengdu, China.

Liu, Y., X. Chang, J. He, F. Liu, and H. Sun (2005), Three-dimensional velocity images of the crust and upper mantle beneath the north-south zone in China, *Bull. Seismol. Soc. Am.*, *95*, 916–925.

Ma, J., M S., L. Liu, T. Liu, and X. Wu (2000), Experimental study on alternate slip of intersecting faults and block movement, *Seismol. Geol.*, *22*, 65–73.

Ma, X. (1989), Lithospheric dynamics atlas of China (in Chinese), China Cartogr. Publ. House, Beijing.

Ma, Z., X. Chen, S. Ye, X. Nai, Z. Wei, J. Chen, J. Ning, H. Xu, and G. Ding (2001), Contemporary crustal movement of continental China obtained by Global Positioning System (GPS) measurements (in Chinese), *Sci. Bull.*, *46*(13), 1118–1120.

Meade, B. J., and B. H. Hager (2005), Block models of crustal motion in southern California constrained by GPS measurements, *J. Geophys. Res.*, *110*, B03403, doi:10.1029/2004JB003209.

Michel, G. W., M. Becker, D. Angermann, C. Reigber, and E. Reinhart (2000), Crustal motion in E- and SE-Asia from GPS measurements, *Earth Planets Space*, *52*, 713–720.

Molnar, P., and P. Tapponnier (1975), Cenozoic tectonics of Asia: effects of a continental collision, *Science*, *189*, 419–426.

Molnar, P., P. England, and J. Martinod (1993), Mantle dynamics, uplift of the Tibetan Plateau, and the Indian monsoon, *Rev. Geophys.*, *31*, 357–396.

Otofuji, Y., Y. Liu, M. Yokoyama, M. Tamai, and J. Yin (1998), Tectonic deformation of the southwestern part of the Yangtze craton inferred from paleomagnetism, *Earth Planets. Sci. Lett.*, *156*, 47–60.

Paul, J., et al. (2001), The motion and active deformation of India, *Geophys. Res. Lett.*, *28*, 647–650.

Peltzer, G., and P. Tapponnier (1988), Formation and evolution of strike-slip faults, rifts, and basins during the India-Asia collision: An experimental approach, *J. Geophys. Res.*, *93*, 15,085–15,117.

Ren, J. (1990), Preliminary study on the recurrence period of strong earthquakes on the fracture zone of Zemuhe, west of Sichuan, *Inland Earthquake*, *4*(2), 107–115.

Replumaz, A., and P. Tapponnier (2003), Reconstruction of the deformed collision zone between India and Asia by backward motion of lithospheric blocks, *J. Geophys. Res.*, *108*(B6), 2285, doi:10.1029/2001JB000661.

Replumaz, A., R. Lacassin, P. Tapponnier, and P. H. Leloup (2001), Large river offsets and Plio-Quaternary dextral slip rate on the Red River fault (Yunnan, China), *J. Geophys. Res.*, *106*, 819–836.

Royden, L. H., B. C. Burchfiel, R. W. King, E. Wang, Z. Chen, F. Shen, and Y. Liu (1997), Surface deformation and lower crustal flow in eastern Tibet, *Science*, *276*, 788–790.

Savage, J. C., and R. O. Burford (1970), Accumulation of tectonic strain in California, *Bull. Seismol. Soc. Am.*, *60*, 1877–1896.

Schärer, U., P. Tapponnier, R. Lacassin, P. H. Leloup, D. L. Zhong, and S. C. Ji (1990), Intraplate tectonics in Asia: A precise age for large-scale Miocene movement along the Ailao Shan-Red River shear zone, China, *Earth Planet. Sci. Lett.*, *97*, 65–77.

Shen, F., L. H. Royden, and B. C. Burchfiel (2001), Large-scale crustal deformation of the Tibetan Plateau, *J. Geophys. Res.*, *106*, 6793–6816.

Shen, Z.-K., C. Zhao, A. Yin, Y. Li, D. D. Jackson, P. Fang, and D. Dong (2000), Contemporary crustal deformation in east Asia constrained by Global Positioning System measurements, *J. Geophys. Res.*, *105*, 5721–5734.

Shen, Z.-K., M. Wang, Y. Li, D. D. Jackson, A. Yin, D. Dong, and P. Fang (2001), Crustal deformation along the Altyn Tagh fault system, western China, from GPS, *J. Geophys. Res.*, *106*, 30,607–30,622.

Tang, R., W. Han, Z. Huang, H. Zian, and Y. Zhang (1993), *Active Faults and Earthquakes in Sichuan Province*, 360 pp., Seismol. Publ. House, Beijing.

Tang, R., Z. Huang, S. Ma, Y. Gong, and R. Zou (1995), Basic characteristics of active fault zones in Sichuan Province, *Seismol. Geol.*, *17*, 390–396.

Tapponnier, P., and P. Molnar (1977), Active faulting and tectonics in China, *J. Geophys. Res.*, *82*, 2905–2930.

Tapponnier, P., G. Peltzer, A. Y. Le Dain, R. Armijo, and P. Cobbold (1982), Propagating extrusion tectonics in Asia: New insights from simple experiments with plasticine, *Geology*, *10*, 611–616.

Tapponnier, P., R. Lacassin, P. H. Leloup, U. Schärer, D. L. Zhong, X. H. Liu, S. C. Ji, L. S. Zhang, and J. Y. Zhong (1990), The Ailao Shan/Red River metamorphic belt: Tertiary left-lateral shear between Indochina and south China, *Nature*, *343*, 431–437.

Tapponnier, P., Z. Xu, F. Roger, B. Meyer, N. Arnaud, G. Wittlinger, and J. Yang (2001), Oblique stepwise rise and growth of the Tibet Plateau, *Science*, *294*, 1671–1677.

Thatcher, W. (1983), Nonlinear strain buildup and the earthquake cycle on the San Andreas fault, *J. Geophys. Res.*, *88*, 5893–5902.

Vigny, C., A. Socquet, C. Rangin, N. Chamot-Rooke, M. Pubellier, M.-N. Bouin, G. Bertrand, and M. Becker (2003), Present-day crustal deformation around Sagaing fault, Myanmar, *J. Geophys. Res.*, *108*(B11), 2533, doi:10.1029/2002JB001999.

Vilotte, J. P., R. Madariaga, M. Daignières, and O. Zienkiewicz (1986), Numerical study of continental collision: Influence of buoyancy forces and initial stiff inclusion, *Geophys. J. R. Astron. Soc.*, *84*, 279–310.

Wang, C.-Y., W. W. Chan, and W. D. Mooney (2003), Three-dimensional velocity structure of crust and upper mantle in southwestern China and its tectonic implications, *J. Geophys. Res.*, *108*(B9), 2442, doi:10.1029/2002JB001973.

Wang, E., and B. C. Burchfiel (1997), Interpretation of Cenozoic tectonics in the right-lateral accommodation zone between the Ailao Shan shear zone and the eastern Himalayan syntaxis, *Int. Geol. Rev.*, *39*, 191–219.

Wang, E., and B. C. Burchfiel (2000), Late Cenozoic to Holocene deformation in southwestern Sichuan and adjacent Yunnan, China, and its role in formation of the southeastern part of the Tibetan Plateau, *Geol. Soc. Am. Bull.*, *112*, 413–423.

Wang, E., B. C. Burchfiel, L. H. Royden, L. Chen, J. Chen, W. Li, and Z. Chen (1998), Late Cenozoic Xianshuihe-Xiaojiang, Red River, and Dali fault systems of southwestern Sichuan and central Yunnan, China, *Spec. Pap. Geol. Soc. Am.*, *327*, 108 pp.

Wang, M., Z.-K. Shen, Z. Niu, Z. Zhang, H. Sun, W. Gan, Q. Wang, and Q. Ren (2003), Contemporary crustal deformation and active blocks model of China mainland (in Chinese), *Sci. China, Ser. D*, *33*(suppl.), 21–32.

Wang, Q., et al. (2001), Present-day crustal deformation in China constrained by Global Positioning System measurements, *Science*, *294*, 574–577.

Weldon, R., K. Sieh, O. Zhu, Y. Han, J. Yang, and S. Robinson (1994), Slip rate and recurrence interval of earthquakes on the Hong He (Red River) fault, Yunnan, PRC, paper presented at International Workshop Seismotectonics and Seismic Hazard in South East Asia, UNESCO, Hanoi.

Wen, X., W. Han, T. Li, Y. Zhou, Y. He, R. Weldon, J. Stimic, and Y. Yang (1996), Slip-rate and recurrence intervals of the Luhuo/Daofu segment of the Xianshuihe fault, Sichuan, PRC, *Eos Trans. AGU*, *77*(46), Fall Meet. Suppl., F693–F694,

Xiang, H., S. Guo, X. Xu, W. Zhang, and X. Dong (2000), Active block division and present-day motion features of the south region of Sichuan-Yunnan Province (in Chinese), *Seismol. Geol.*, *22*, 253–264.

Xiang, H., X. Xu, S. Guo, W. Zhang, H. Li, and G. Yu (2002), Sinistral thrusting along the Lijiang-Xiaojinhe fault since Quaternary and its geologic-tectonic significance—Shielding effect of transverse structure of intracontinental active block (in Chinese), *Seismol. Geol.*, *24*, 188–198.

Xu, G., and P. J. J. Kamp (2000), Tectonics and denudation adjacent to the Xianshuihe fault, eastern Tibetan Plateau: Constraints from fission track thermochronology, *J. Geophys. Res.*, *105*, 19,231–19,251.

Xu, X., X. Wen, R. Zheng, W. Ma, F. Song, and G. Yu (2003), Pattern of latest tectonic motion and dynamics of faulted blocks in Yunnan and Sichuan (in Chinese), *Sci. China, Ser. D*, *33*(suppl.), 151–162.

Yang, Z., Y. Chen, Y. Zheng, and X. Yu (2003), Application of the double difference earthquake relocation method to the earthquakes of central and western China (in Chinese), *Sci. China, Ser. D*, *33*(suppl.), 130–134.

Yin, A., and T. M. Harrison (2000), Geologic evolution of the Himalayan-Tibetan orogen, *Annu. Rev. Earth Planet Sci.*, *28*, 211–280.

Yoshioka, S., Y. Liu, K. Sato, H. Inokuchi, L. Su, H. Zaman, and Y. Otofuji (2003), Paleomagnetic evidence for post-Cretaceous internal deformation of the Chuan Dian Fragment in the Yangtze block: A consequence of indentation of India into Asia, *Tectonophysics*, *376*, 61–74.

Zhang, C., F. Xie, and S. Zhang (2001), A modeling study on the controlling factors of seismic source distribution and their strength index—Practical analyses of the seismic environmental factors of the Red River fault (in Chinese), *Acta Seismol. Sin.*, *23*(2), 125–135.

Zhang, L. S., and U. Schärer (1999), Age and origin of magmatism along the Cenozoic Red River shear belt, China, *Contrib. Mineral. Petrol.*, *134*, 67–85.

Zhang, P., et al. (2004), Continuous deformation of the Tibetan Plateau from global positioning system data, *Geology*, *32*, 809–812.

Zhang, S., and F. Xie (2001), Seismo-tectonic divisions of strong earthquakes ($M_s \geq 7.0$) and their tectonic Geomorphology along Xianshuihe-Xiaojiang fault zone (in Chinese), *Acta Seismol. Sin.*, *23*(1), 36–44.

R. Bürgmann, Department of Earth and Planetary Science, University of California, Berkeley, CA 94720-4760, USA.

J. Lü, Department of Geophysics, Peking University, Beijing, 100871 China.

Z.-K. Shen, Department of Earth and Space Sciences, University of California, Los Angeles, CA 90095-1567, USA. (zshen@noah.ess.ucla.edu)

M. Wang, Institute of Earthquake Science, China Earthquake Administration, Beijing, 100036 China.